Visualization of intracellular ATP dynamics in different nephron segments under pathophysiological conditions using the kidney slice culture system

see commentary on page 362

OPEN

Shigenori Yamamoto[1,2], Shinya Yamamoto[1], Masahiro Takahashi[1], Akiko Mii[1,7], Akihiro Okubo[1], Naoya Toriu[1,2], Shunsaku Nakagawa[3], Takaaki Abe[4], Shingo Fukuma[5], Hiromi Imamura[6], Masamichi Yamamoto[1,8] and Motoko Yanagita[1,2]

[1]Department of Nephrology, Graduate School of Medicine, Kyoto University, Kyoto, Japan; [2]Institute for the Advanced Study of Human Biology (WPI-ASHBi), Kyoto University, Kyoto, Japan; [3]Department of Clinical Pharmacology and Therapeutics, Kyoto University Hospital, Kyoto, Japan; [4]Department of Clinical Biology and Hormonal Regulation, Tohoku University Graduate School of Medicine, Sendai, Japan; [5]Department of Human Health Sciences, Graduate School of Medicine, Kyoto University, Kyoto, Japan; and [6]Graduate School of Biostudies, Kyoto University, Kyoto, Japan

ATP depletion plays a central role in the pathogenesis of kidney diseases. Recently, we reported spatiotemporal intracellular ATP dynamics during ischemia reperfusion (IR) using GO-ATeam2 mice systemically expressing an ATP biosensor. However, observation from the kidney surface did not allow visualization of deeper nephrons or accurate evaluation of ATP synthesis pathways. Here, we established a novel ATP imaging system using slice culture of GO-ATeam2 mouse kidneys, evaluated the ATP synthesis pathway, and analyzed intracellular ATP dynamics using an *ex vivo* IR-mimicking model and a cisplatin nephropathy model. Proximal tubules (PTs) were found to be strongly dependent on oxidative phosphorylation (OXPHOS) using the inhibitor oligomycin A, whereas podocytes relied on both OXPHOS and glycolysis using phloretin an active transport inhibitor of glucose. We also confirmed that an *ex vivo* IR-mimicking model could recapitulate ATP dynamics *in vivo*; ATP recovery in PTs after reoxygenation varied depending on anoxic time length, whereas ATP in distal tubules (DTs) recovered well even after long-term anoxia. After cisplatin administration, ATP levels in PTs decreased first, followed by a decrease in DTs. An organic cation transporter 2 inhibitor, cimetidine, suppressed cisplatin uptake in kidney slices, leading to better ATP recovery in PTs, but not in DTs. Finally, we confirmed that a mitochondria protection reagent (Mitochonic Acid 5) delayed the cisplatin-induced ATP decrease in PTs. Thus, our novel system may provide new insights into the energy dynamics and pathogenesis of kidney disease.

Kidney International (2024) **106,** 470–481; https://doi.org/10.1016/j.kint.2024.05.028

KEYWORDS: AKI; ATP; cisplatin nephropathy; energy dynamics; imaging; mitochondria

Translational Statement

Our novel system enabled visualization of intracellular adenosine-5'-triphosphate dynamics in various kidney cells, including deeper nephron segments. Kidney slices retain a 3-dimensional structure and a high degree of *in vivo* cellular functionality and can respond to disease models as *in vivo*. This system is easy to use for controlled intervention experiments. In addition, it allows multiple slices to be cultured from a single kidney and various experimental conditions to be tested, which is appropriate from an animal welfare perspective. This system could be a powerful tool for evaluating the nephrotoxicity of new drugs and promoting drug discovery that improves energy dynamics.

The kidney consumes a large amount of adenosine-5'-triphosphate (ATP). ATP is produced by glycolysis and mitochondrial oxidative phosphorylation (OXPHOS).[1] Mitochondrial damage not only causes energy depletion but also results in renal fibrosis through an inflammatory response[2,3] and has been reported in common diseases such as acute kidney injury and drug-induced kidney injury.[1] Therefore, insights into kidney energy metabolism are crucial for understanding the mechanism of kidney disease.

Correspondence: *Motoko Yanagita, Department of Nephrology, Graduate School of Medicine, Kyoto University, Shogoin-Kawahara-cho 54, Sakyo-ku, Kyoto 606-8507, Japan. E-mail: motoy@kuhp.kyoto-u.ac.jp*

[7]Current address: Department of Endocrinology, Metabolism and Nephrology, Graduate School of Medicine, Nippon Medical School, Tokyo, Japan.

[8]Current address: Department of Research Promotion and Management, National Cerebral and Cardiovascular Center, Osaka, Japan.

Received 15 October 2023; revised 11 April 2024; accepted 24 May 2024; published online 9 July 2024

Recently, we revealed the difference in intracellular ATP dynamics between proximal tubules (PTs) and distal tubules (DTs) during ischemia reperfusion (IR) injury using 2-photon microscopy and GO-ATeam2 mice, which enabled the visualization of intracellular ATP dynamics at a single-cell level.[4]

However, *in vivo* ATP imaging techniques have some critical limitations. First, deeper kidney regions cannot be observed from the kidney surface because the imaging depth of 2-photon microscopy in the kidney is only 150 μm. Second, ATP synthesis inhibitors cannot be used in *in vivo* experiments because of their significant effects on circulation.

In this study, we established a novel *ex vivo* observation system using a slice culture of GO-ATeam2 mouse kidneys, which enabled visualization of intracellular ATP dynamics in various kidney cells, including deeper nephron segments.

METHODS

The kidneys of GO-ATeam2 mice were immediately sliced at 300 μm using a tissue slicer in ice-cold buffer containing

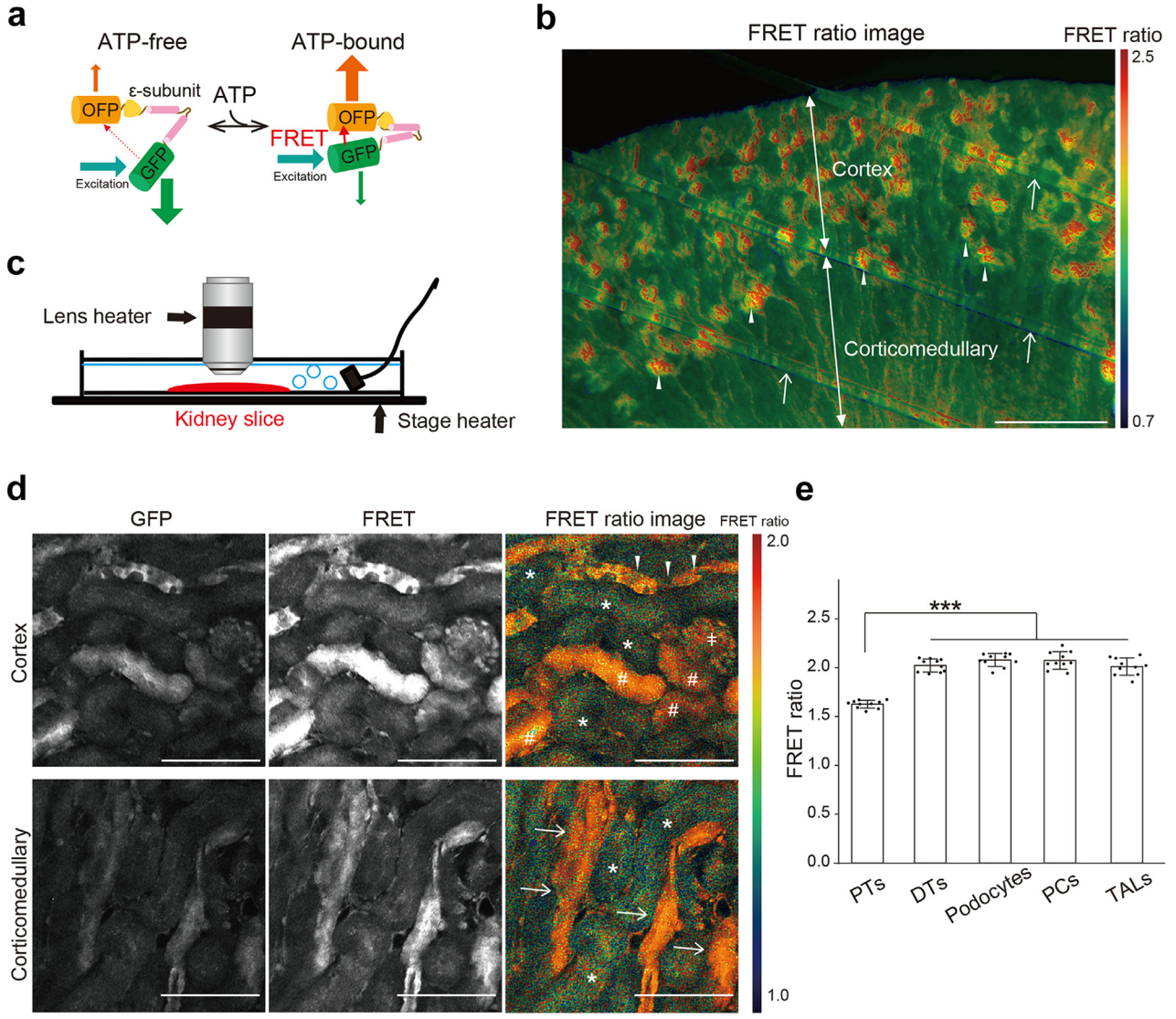

Figure 1 | Establishment of the novel adenosine-5'-triphosphate (ATP) imaging system using a kidney slice culture. (**a**) Schematic drawing of the ATP fluorescence resonance energy transfer (FRET) biosensor. The ATP FRET biosensor changes its structure depending on the intracellular ATP concentrations. (**b**) ATP distribution shown by the ratio image of FRET/green fluorescent protein (GFP) emission in kidney slices using fluorescence stereomicroscopy. The arrowheads indicate glomeruli, and the arrows indicate slice anchor strings. (**c**) Schematic drawing of the ATP imaging system using a kidney slice culture and 2-photon microscopy. Briefly, 300-μm-thick kidney slices from GO-ATeam2 mice were placed into a chamber and secured with a slice anchor. (**d**) Visualization of intracellular ATP levels in proximal tubules (PTs*), distal tubules (DTs#), glomeruli‡, collecting ducts (CDs; arrowheads), and thick ascending limbs (TALs; arrows). (**e**) FRET ratios (FRET/GFP) in PTs, DTs, podocytes, principal cells (PCs) and TALs (n = 10 slices). Statistical significance among nephron segments was assessed using 1-way analysis of variance with Tukey-Kramer *post hoc* tests for comparisons. ***$P < 0.001$. Bar = (**b**) 500 μm and (**d**) 100 μm. To optimize viewing of this image, please see the online version of this article at www.kidney-international.org.

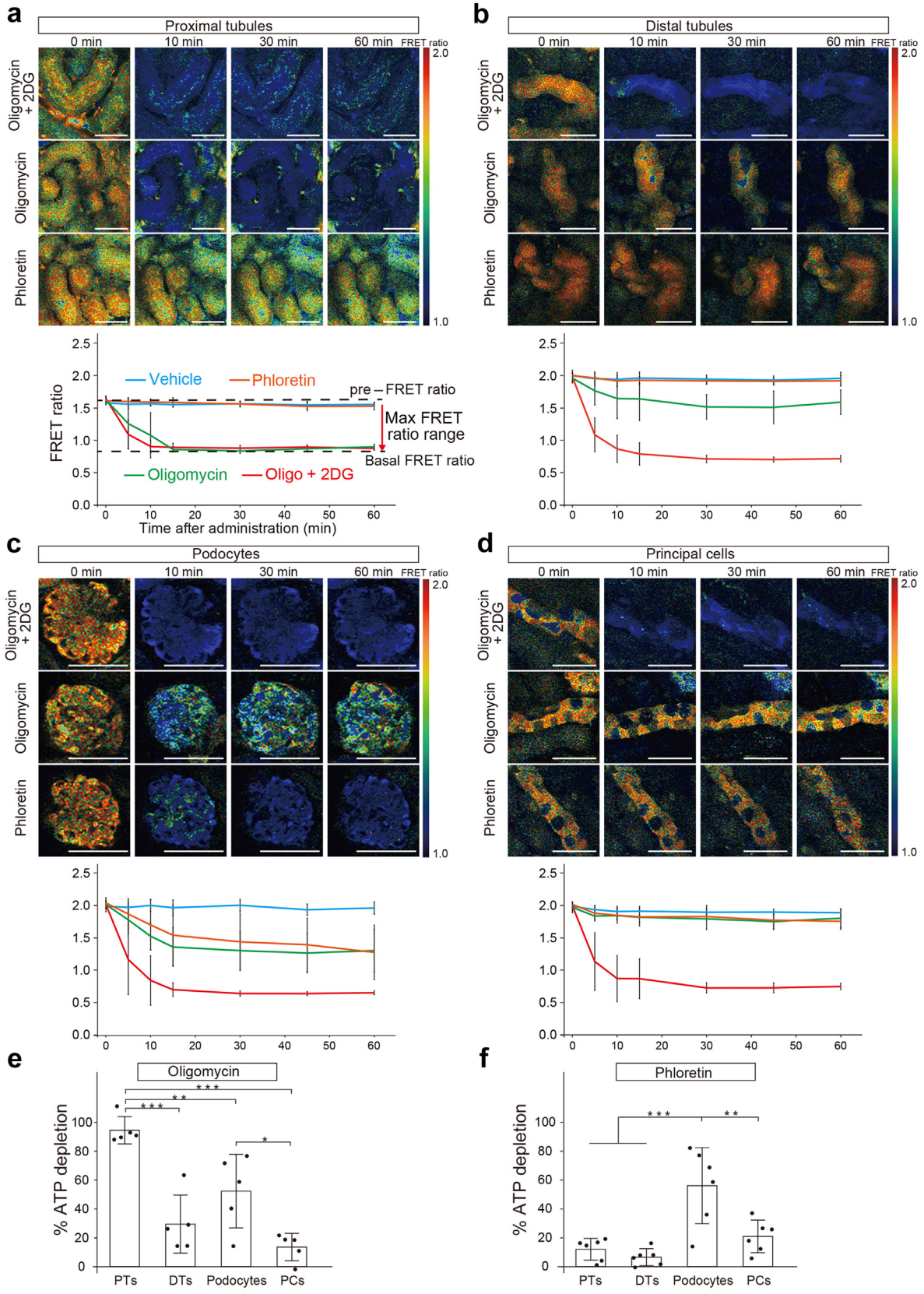

Figure 2 | Intracellular adenosine-5'-triphosphate (ATP) levels in various nephron segment after the administration of ATP synthesis inhibitors. (**a–d**) Fluorescence resonance energy transfer (FRET) ratio images in various nephron segments after the administration of oligomycin and 2-deoxy-D-glucose (2DG; upper rows), oligomycin alone (middle rows), and phloretin alone (lower rows). Trends of FRET ratios are shown in graphs for each nephron segment after the administration of oligomycin and 2DG (red; n = 5 slices), oligomycin (continued)

glucose and sodium pyruvate, gassed with 95% O_2 and 5% CO_2. Kidney slices were placed in our original chamber, in the same buffer, and secured using a slice anchor. To confirm the viability of the kidney cells, we performed the ATP imaging and the morphological evaluation at longer time points after the kidney slice preparation (Supplementary Figure S1). We identified each nephron segment by immunostaining analysis (Supplementary Figure S2). Full methods, including mouse treatment, histologic analysis, and the sequences of primers for real-time polymerase chain reaction (Supplementary Table S1), are available in the Supplementary Methods.

RESULTS

Establishment of the novel ATP imaging system with kidney slice culture

We prepared kidney slices from GO-Ateam2 mice, which expressed ATP biosensor systemically (Figure 1a), and established an *ex vivo* ATP imaging system that allowed us to simultaneously observe various nephron segments using fluorescence stereomicroscopy (Figure 1b). Detailed images were obtained using 2-photon microscopy (Figure 1c and d). Warm colors indicate high fluorescence resonance energy transfer (FRET) ratios (high ATP levels) and cool colors indicate low FRET ratios (low ATP levels; Figure 1b and d). The FRET ratios in various segments (Figure 1e) were similar to those *in vivo*,[4] suggesting that the energy metabolism similar to that *in vivo* might be maintained in this system.

Intracellular ATP dynamics after ATP synthesis inhibitor administration

To inhibit ATP synthesis, we applied oligomycin A (oligomycin), an OXPHOS inhibitor; 2-deoxy-D-glucose (2DG), a glycolytic inhibitor; and phloretin, a glucose transporter inhibitor to kidney slices. Although there was no apparent ATP change in vehicle-treated controls for 60 minutes (Supplementary Figure S3), simultaneous administration of oligomycin (20 μM) and 2DG (20 mM) decreased ATP levels in all segments to basal levels within approximately 10 minutes (Figure 2a–d). After administering oligomycin (20 μM) alone, the ATP decline rate and plateau levels in PTs were similar to those observed after the simultaneous administration of oligomycin and 2DG (Figure 2a and e), indicating a high dependence of PTs on OXPHOS. Conversely, ATP levels in DTs and principal cells decreased slowly and moderately (Figure 2b, d, and e). In podocytes, oligomycin administration reduced ATP levels to some extent (Figure 2c and e), suggesting that podocytes require moderate OXPHOS for ATP synthesis. However, 2DG (20 mM) administration alone did not cause any marked changes in any segment. Even at a concentration of 100 mM, ATP levels in podocytes decreased slightly (Supplementary Figure S4). Instead, we administered phloretin (100 μM) and found that podocytes, but not the other segments, showed a significant reduction in ATP levels (Figure 2c and f). This finding indicates that podocytes actively take up glucose via glucose transporters and use both OXPHOS and glycolysis for ATP synthesis.

An *ex vivo* IR-mimicking model recapitulates intracellular ATP dynamics for *in vivo* IR injury

To confirm whether this novel *ex vivo* system could recapitulate intracellular ATP dynamics in kidney diseases, we first induced culture conditions that mimicked IR injury[5,6] (Figure 3a). The ATP levels in both PTs and DTs decreased rapidly to basal levels after 30 minutes of anoxia but recovered differently after reoxygenation (Figure 3b, c, and e). ATP in PTs after reoxygenation recovered insufficiently, whereas ATP in DTs recovered almost completely, indicating the resistance of DTs to IR injury. We also found that a longer anoxic time resulted in poorer ATP recovery (Figure 3b, d, and e) and severer histologic damage in PTs (Figure 4), and induced gene expression changes reflecting inflammatory response and metabolic changes (Supplementary Figure S5). Taken together, this system could recapitulate intracellular ATP dynamics during IR injury *in vivo*.[4] We also evaluated intracellular ATP dynamics of PTs in the corticomedullary region in this model, which could not be observed *in vivo* observation from the kidney surface. Whereas the FRET ratio in PTs in the corticomedullary region was slightly lower than that in PTs in the cortex, intracellular ATP dynamics and the % ATP recovery were comparable between the groups (Supplementary Figure S6).

ATP levels decrease both in PTs and DTs in a cisplatin nephropathy model

In a cisplatin nephropathy model *in vivo*, we found ATP-depleted degenerated tubules and mitochondrial damages using electron microscopy and tetramethyl rhodamine methyl ester analysis (Figure 5). However, it was still unclear which nephron segments were damaged due to severe injury. To answer this question, we evaluated the sensitivity of various nephron segments to cisplatin using this system. After cisplatin administration, ATP levels decreased mainly in PTs and DTs but not in podocytes or principal cells (Figure 6).

Cisplatin nephrotoxicity is mediated via OCT2 in PTs but not in DTs in an *ex vivo* system

Cisplatin accumulates within the tubules via organic cation transporter 2 (OCT2), which is specifically expressed in

Figure 2 | (continued) alone (green; n = 5 slices), phloretin alone (orange; n = 6 slices), and vehicle control (blue; n = 4 slices). The ATP level in all segments reached the basal level after the administration of oligomycin and 2DG. The maximum FRET ratio range in each segment is defined as follows: (pre–FRET ratio) − (basal FRET ratio after the administration of oligomycin and 2DG). (**e,f**) The % ATP depletion after the administration of oligomycin alone and phloretin alone in each nephron segment was shown. The % ATP depletion was defined as follows: [(pre–FRET ratio) − (FRET ratio after the administration of each inhibitor for 60 min)] × 100 (%) / (maximum FRET ratio range). Statistical significance among nephron segments was assessed using 1-way analysis of variance with Tukey-Kramer *post hoc* tests for comparisons. *$P < 0.05$; **$P < 0.01$; ***$P < 0.001$. Bar = 50 μm. DT, distal tubule; PC, principal cell; PT, proximal tubule. To optimize viewing of this image, please see the online version of this article at www.kidney-international.org.

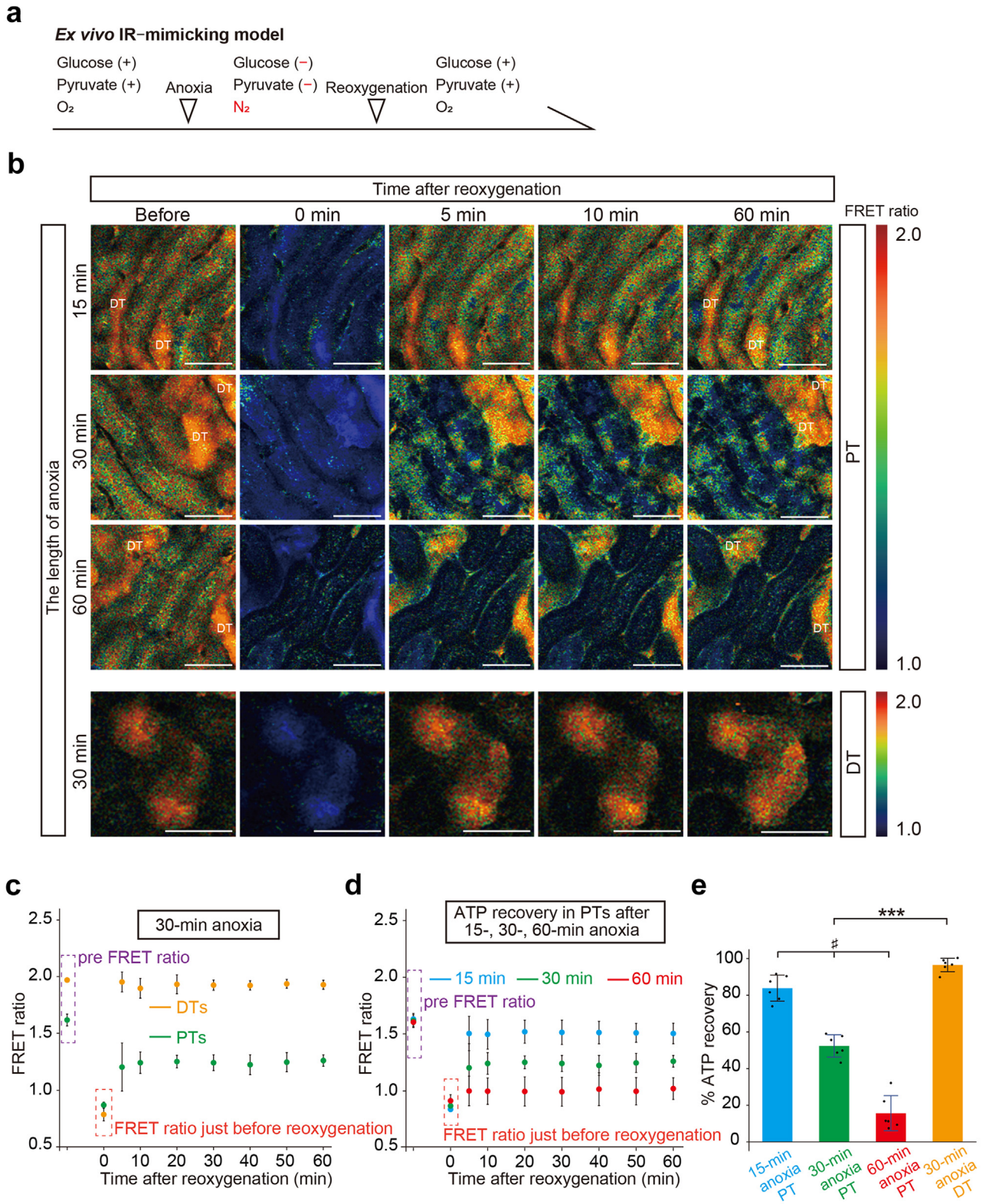

Figure 3 | Adenosine-5'-triphosphate (ATP) recovery in proximal tubules (PTs) varies depending on the length of anoxia in an *ex vivo* IR-mimicking model. (**a**) Schematic drawing of the *ex vivo* ischemia reperfusion–mimicking model. (**b**) Fluorescence resonance energy transfer (FRET) ratio images of PTs during reoxygenation after 15-, 30-, and 60-minute anoxia and those of distal tubules (DTs) after 30-minute anoxia. (**c**) FRET ratio graph of PTs (green) and DTs (yellow) during reoxygenation after 30-minute anoxia (n = 6 slices). (**d**) FRET ratio graph of PTs during reoxygenation after 15-, 30-, and 60-minute anoxia (blue, green, and red, respectively; n = 6 kidney slices per groups). FRET ratio graph of PTs after 30-minute anoxia in (**c**) is presented here again. (**e**) The % ATP recovery is defined as follows: [(FRET ratio 60 min after reoxygenation) − (FRET ratio just before reoxygenation)] × 100 (%) / {(pre–FRET ratio) − (FRET ratio just before reoxygenation)}. Statistical significance was assessed using a trend test across 15-, 30-, and 60-minute anoxia groups. Differences between the 2 groups (30-minute anoxia PT vs. 30-minute anoxia DT) were compared using an unpaired, 2-tailed *t* test. #*P* for trend < 0.001; ***$P < 0.001$. Bar = 50 μm. To optimize viewing of this image, please see the online version of this article at www.kidney-international.org.

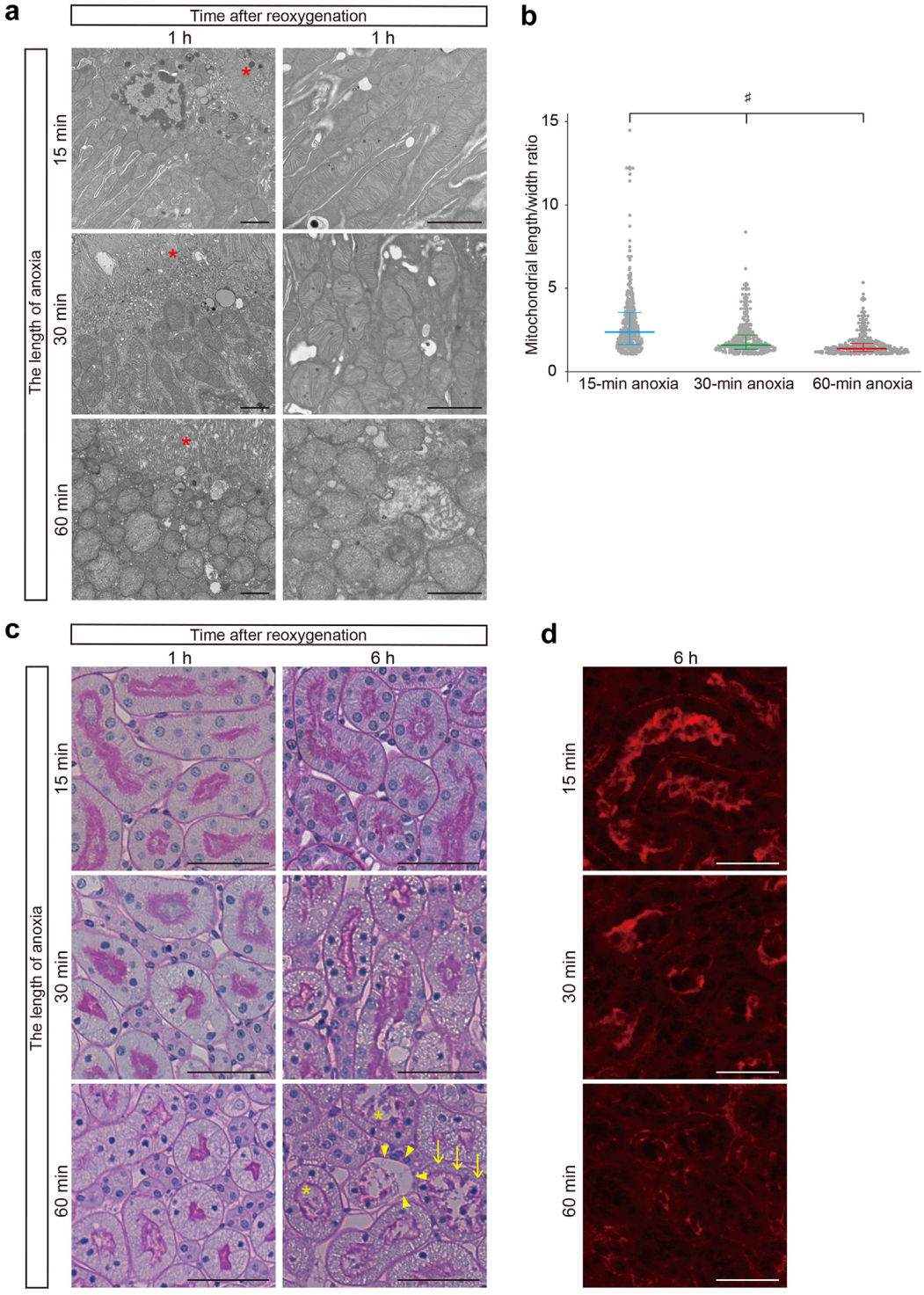

Figure 4 | Histologic changes in an *ex vivo* ischemia reperfusion–mimicking model. (**a**) At 1 hour after reoxygenation, electron microscopy analysis showed that a longer anoxic time resulted in more pronounced changes in the mitochondrial structures in proximal tubules (PTs). *Brush borders. (**b**) Quantitative evaluation was performed using the mitochondrial length/width ratio (n = 3 slices, 9 tubules, 450 mitochondria). (**c**) Periodic acid–Schiff staining of the kidney slices 1 hour and 6 hours after reoxygenation. At 1 hour after reoxygenation, no apparent histologic injury or only a minor change was observed, even in the slices that underwent 60-minute anoxia. At 6 hours after reoxygenation, tubular injuries, such as tubular epithelial shedding (arrowheads), debris*, and brush border loss (arrows), were observed in the slices that underwent a longer anoxia. Representative images are shown. (**d**) Immunostaining of the slices 6 hours after 15-, 30-, and 60-minute anoxia. Positive phalloidin staining indicates brush borders in PTs. A healthy tall brush border was maintained in kidney slices that underwent 15-minute anoxia, whereas a shedding or shortened brush border was observed in the slices that underwent 60-minute anoxia. Representative images are shown. Statistical significance was assessed using a trend test across 15-, 30-, and 60-minute anoxia groups (**b**). #*P* for trend < 0.001. Bar = (**a**) 2 μm, (**c**) 50 μm, and (**d**) 25 μm. To optimize viewing of this image, please see the online version of this article at www.kidney-international.org.

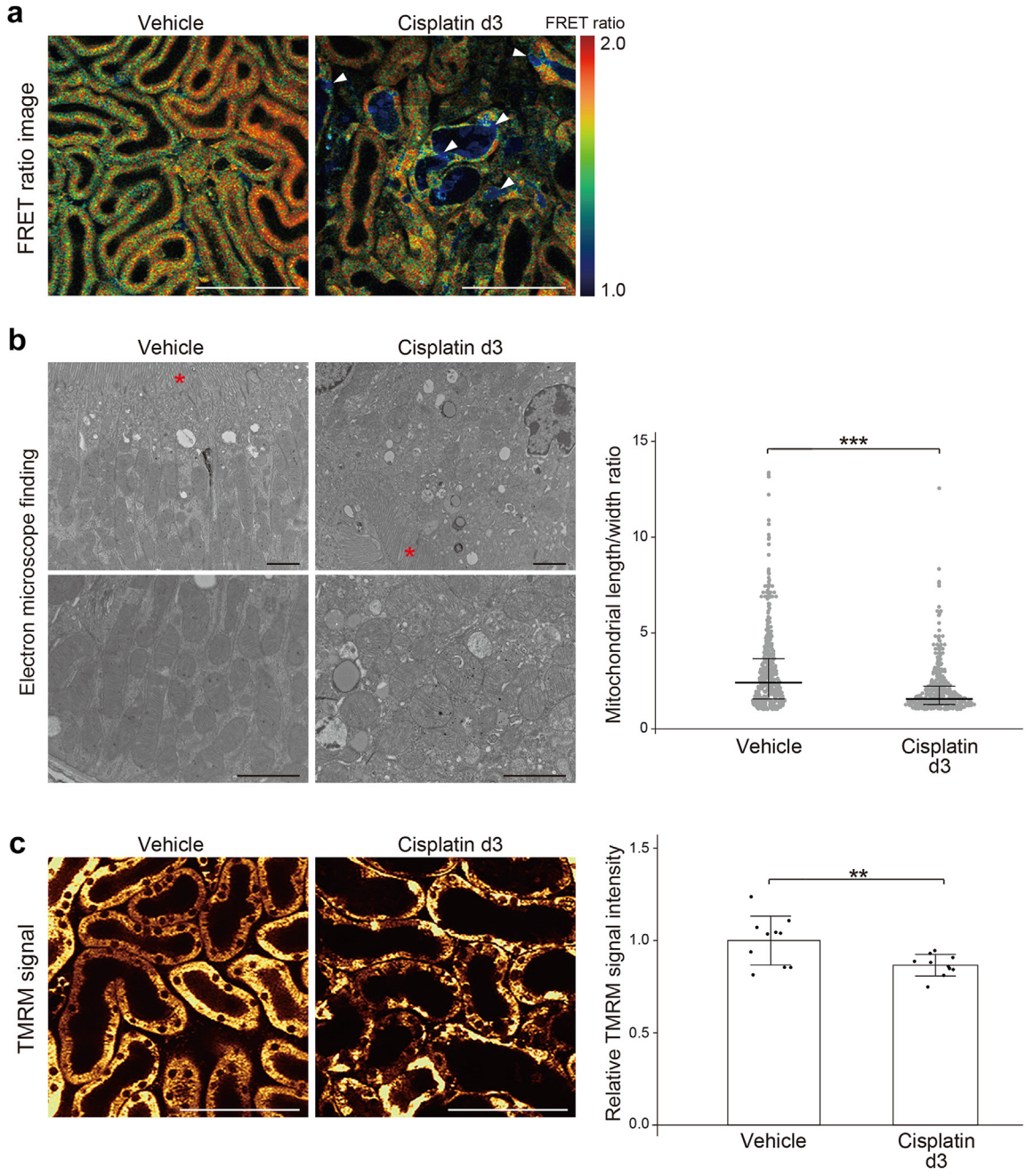

Figure 5 | Mitochondrial dysfunction and adenosine-5'-triphosphate (ATP) depletion in cisplatin nephropathy *in vivo*. (**a**) Fluorescence resonance energy transfer (FRET) ratio images in living kidneys of mice that were administered cisplatin. Mice were administered 15 mg/kg of cisplatin or vehicle i.p. 3 days before the observation. In the cisplatin group, ATP-depleted cells (arrowheads) were detected in damaged tubules and debris was confirmed in the lumens. Identification of the segments was technically challenging because of the morphological changes. (**b**) Mitochondrial damage was detected in proximal tubules (PTs) of the cisplatin group. Quantitative evaluation was performed using the mitochondrial length/width ratio (n = 3 mice, 9 tubules, 450 mitochondria). *Brush borders. (**c**) Mitochondrial membrane potential shown by the administration of tetramethyl rhodamine methyl ester (TMRM) was reduced in the kidneys of cisplatin-treated mice (n = 3 mice, total of 10 views in each group). Statistical significance was assessed using an unpaired 2-tailed *t* test. $^{**}P < 0.01$; $^{***}P < 0.001$. Bar = (**a**,**c**) 100 μm and (**b**) 2 μm. To optimize viewing of this image, please see the online version of this article at www.kidney-international.org.

PTs,[7,8] explaining its nephrotoxicity in PTs. In our analysis, however, ATP levels in DTs were also reduced. Indeed, we confirmed that DTs were also injured in the cisplatin nephropathy model *in vivo* (Supplementary Figure S7). Therefore, we examined the mechanisms of ATP depletion in PTs and DTs using this system. First, the expression levels of OCT2 protein and mRNA in kidney slices were comparable to those in whole kidneys (Figure 7a and b). Next, the inductively coupled plasma–mass spectrometry method confirmed that cisplatin was taken up by the slices, which was attenuated by 1.0 mM cimetidine, an OCT2 inhibitor[9,10] (Figure 7c). The mitochondrial length/width ratio of PTs was reduced by the

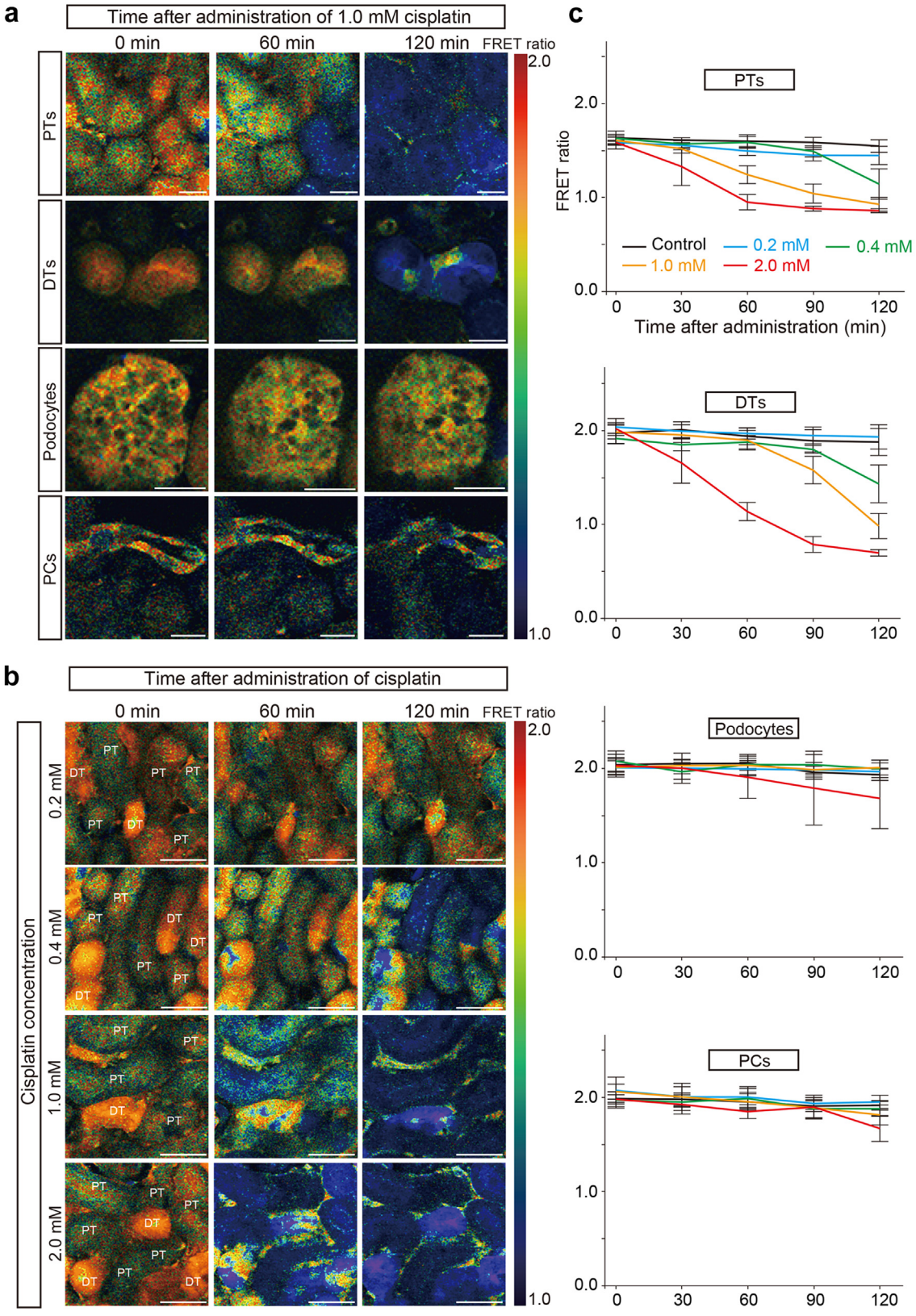

Figure 6| Sensitivity to cisplatin differs among the nephron segments. (**a**) Fluorescence resonance energy transfer (FRET) ratio images after the administration of 1.0 mM cisplatin. During 120 minutes of observation, adenosine-5'-triphosphate levels in proximal tubules (PTs) and distal tubules (DTs), but not those in podocytes and principal cells (PCs), decreased significantly. (**b**) FRET ratio images after the administration of different concentrations of cisplatin. (**c**) FRET ratio graphs after the administration of different concentrations of cisplatin (n = 5 slices in 0.2 mM, 0.4 mM, 1.0 mM groups and n = 6 slices in control and 2.0 mM groups). Bar = (**a**) 25 μm and (**b**) 50 μm. To optimize viewing of this image, please see the online version of this article at www.kidney-international.org.

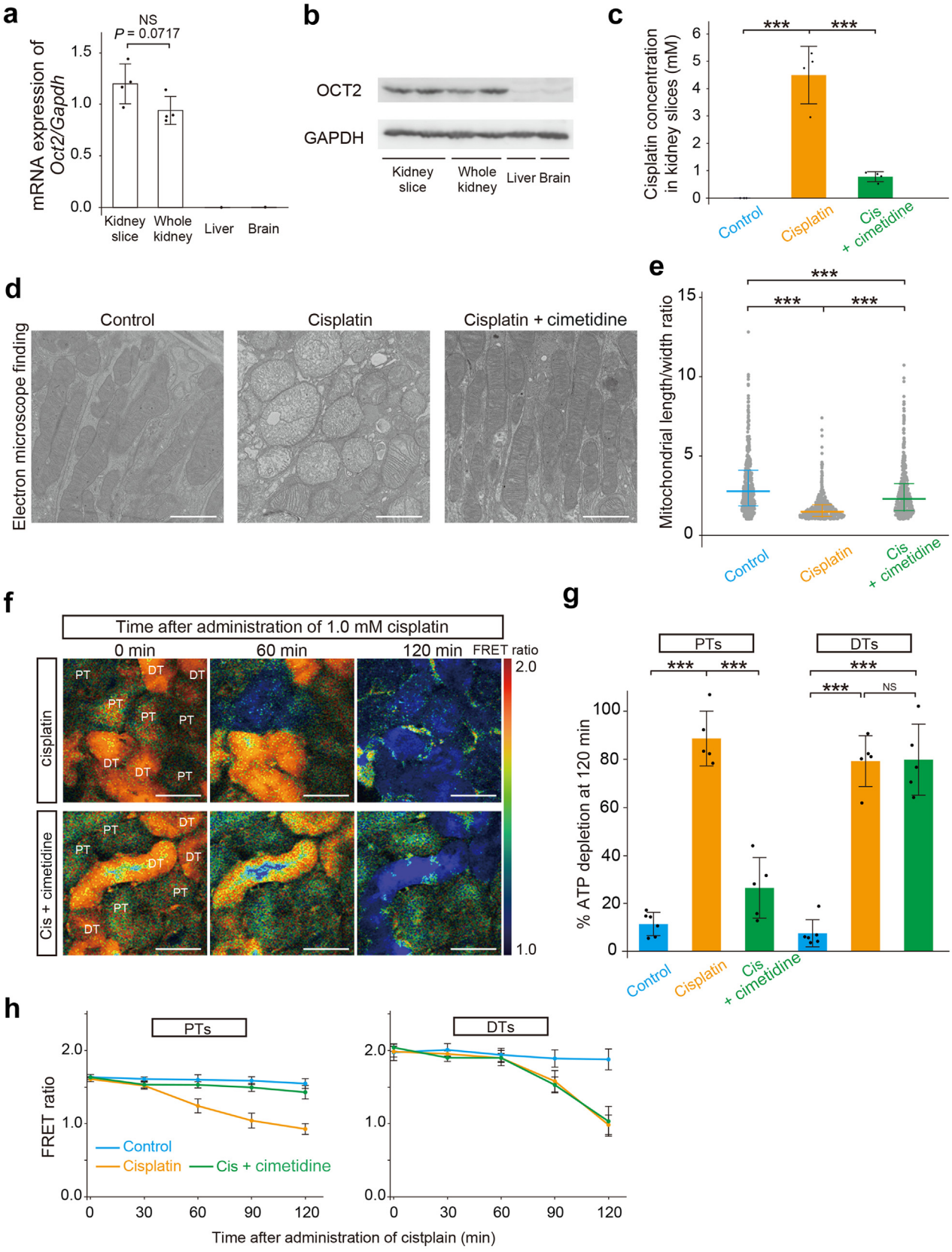

Figure 7 | Cisplatin nephrotoxicity in proximal tubules (PTs), but not that in distal tubules (DTs), is organic cation transporter 2 (OCT2)–mediated. (**a**,**b**) *OCT2* mRNA and OCT2 protein expression levels in kidney slices. Both levels were similar between kidney slices and whole kidneys (n = 4 per group in **a**). Mouse liver and brain samples were used as negative controls. (**c**) The amount of cisplatin uptake in kidney slices was determined using the inductively coupled plasma–mass spectrometry method with or without cimetidine (an (continued)

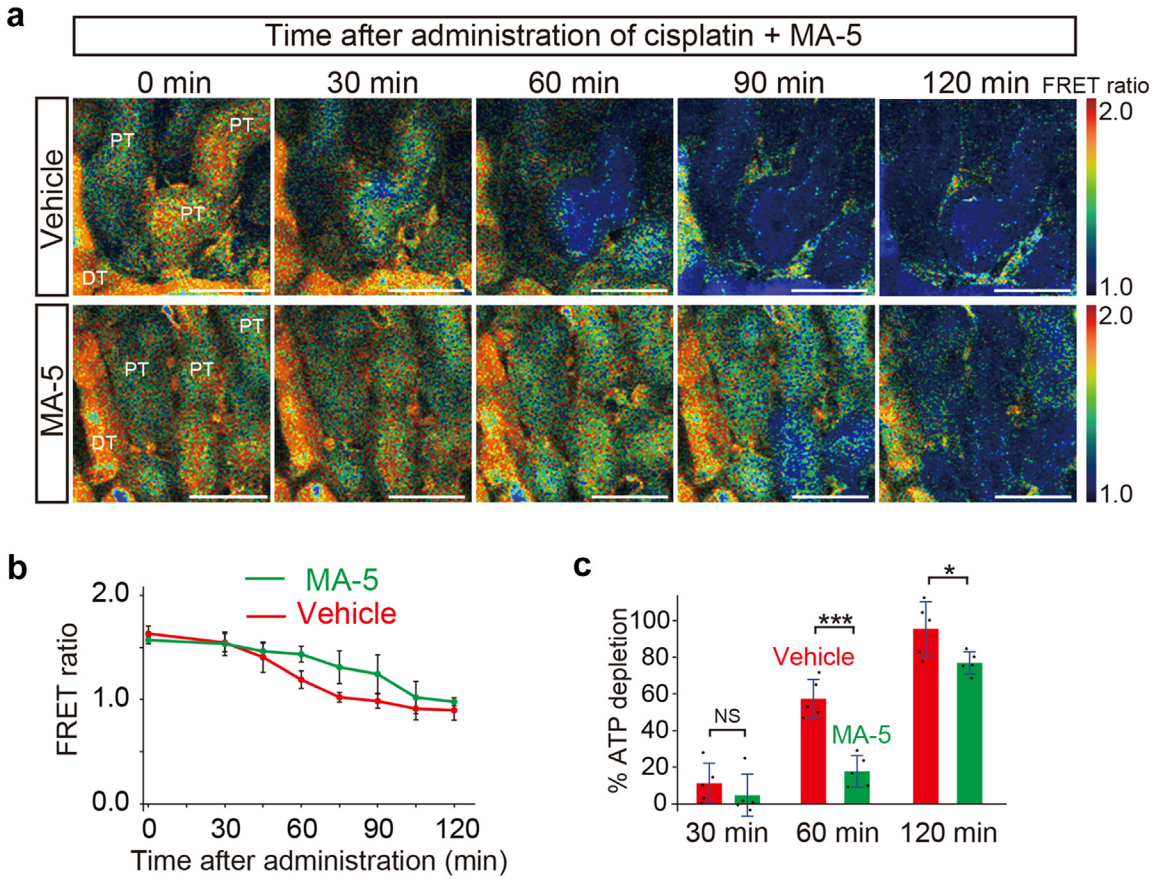

Figure 8 | Mitochonic acid 5 (MA-5) treatment ameliorates adenosine-5'-triphosphate (ATP) depletion induced by cisplatin. (**a**) Fluorescence resonance energy transfer (FRET) ratio images after the administration of cisplatin and MA-5 or vehicle. (**b**,**c**) FRET ratio graphs in proximal tubules (PTs) during 120 minutes of observation (**b**) and the % ATP depletion in PTs 30, 60 and 120 minutes after the administration of reagents (**c**) (n = 5 slices per group). Statistical significance was assessed using an unpaired 2-tailed *t* test. *$P < 0.05$; ***$P < 0.001$; NS, not significant. Bar = 50 μm. To optimize viewing of this image, please see the online version of this article at www.kidney-international.org.

administration of cisplatin, which was reversed by cimetidine (Figure 7d and e). Furthermore, cimetidine ameliorated cisplatin-induced ATP depletion in PTs but not in DTs (Figure 7f–h). These results indicate that the mechanism of DT injury in cisplatin nephropathy may be OCT2 independent. Finally, we examined whether this system could be useful for testing candidate drugs for mitochondrial protection. Mitochonic acid 5 (100 μM), a mitochondria protection reagent,[11,12] ameliorated ATP depletion induced by cisplatin compared with the vehicle group for as long as 120 minutes (Figure 8).

DISCUSSION

Using this novel system, we directly demonstrated ATP synthesis pathways in various nephron segments. The lack of an effect of 2DG was surprising. We speculate that the reasons for this are as follows: (i) previous studies have shown that when one ATP synthesis pathway is inhibited, ATP synthesis is compensated by other pathways, and it is possible that compensation by OXPHOS is observed. (ii) Only hexokinase 1–3, but not glucokinase (hexokinase 4), are inhibited by 2DG. The reason why phloretin was effective but not 2DG in podocytes may be the relatively high expression of

Figure 7 | (continued) OCT2 inhibitor; n = 3 slices in the control group and n = 4 slices in the cisplatin [1.0 mM] and the cisplatin [1.0 mM] + cimetidine [1.0 mM] groups). (**d**) Mitochondrial morphological changes were obvious in PTs in the cisplatin group, which was attenuated in PTs in the cisplatin + cimetidine group. (**e**) Quantitative evaluation of mitochondria morphology using the mitochondrial length/width ratio (n = 3 slices, 9 tubules, 450 mitochondria per each group). (**f**) Fluorescence resonance energy transfer (FRET) ratio images after the administration of cisplatin and cimetidine. (**g**,**h**) FRET ratio graphs in PTs and DTs during 120 minutes of observation (**h**) and the % adenosine-5'-triphosphate (ATP) depletion in PTs and DTs 120 minutes after the administration of reagents (**g**). FRET ratio graphs in the control and 1.0 mM cisplatin groups in Figure 6c are presented again for comparison (n = 5 slices per group). Statistical significance was assessed using 1-way analysis of variance with Tukey-Kramer *post hoc* tests (**c**,**e**,**h**) or an unpaired 2-tailed *t* test (**a**) for comparisons. ***$P < 0.001$; NS, not significant. Bar = (**d**) 2 μm and (**f**) 50 μm. GAPDH, glyceraldehyde-3-phosphate dehydrogenase. To optimize viewing of this image, please see the online version of this article at www.kidney-international.org.

glucokinase in podocytes, according to the KIT (Kidney Interactive Transcriptomics) database.[13] (iii) Most previous studies on kidney metabolism have been conducted *in vitro*, and the baseline metabolic state could be considerably shifted toward the glycolytic system. On the other hand, our novel *ex vivo* system appears to recapitulate the metabolic state *in vivo*, which may make 2DG less effective than in *in vitro* experiments.

Using an *ex vivo* IR-mimicking model, we confirmed that intracellular ATP dynamics of PTs in the corticomedullary region were similar to those of PTs in the cortex, whereas in a mouse IR model, PTs in the corticomedullary region were reported to be the most susceptible.[14,15] This discrepancy might be due to a lack of blood flow[16–18] in this *ex vivo* system, and the reported vulnerability of PTs in the corticomedullary region could be due, at least partly, to hemodynamic alterations rather than in segment-specific metabolic properties.

Furthermore, we, for the first time, found ATP decline in both PTs and DTs in a cisplatin nephropathy model. We also demonstrated that an OCT2 inhibitor canceled ATP decline in PTs but not in DTs. These findings make it plausible to assume that ATP decline in DTs is not a secondary impairment after PT injury.

Our present study has several technical limitations as follows: (i) it is challenging to avoid cellular damage completely during the preparation of kidney slices. At a very low frequency of 2% or less, there were the slices that showed apparently reduced ratios (<1.0) in many segments, and therefore, those slices were excluded from the analysis. (ii) Although the kidney, especially the medullary region, is hypoxic *in vivo*,[19,20] aeration is required in this system (Supplementary Figure S8). However, even under aeration, ATP dynamics in each segment were very similar to those *in vivo*. (iii) This system lacks blood and urine flow, influencing disease progression *in vivo*. Despite these limitations, analysis using this novel ATP imaging system provides valuable information leading to a new understanding of kidney disease mechanisms.

DISCLOSURE

ShigY was employed by the TMK Project, which was a collaborative project between Kyoto University and Mitsubishi Tanabe Pharma. MYan has received research grants from Mitsubishi Tanabe Pharma and Boehringer Ingelheim. MYam has received research grants from Boehringer Ingelheim and Meiji Holdings. All the other authors declared no competing interests.

DATA STATEMENT

All data are available in the main text or the Supplementary Material. We will share the data of this study upon appropriate requests. Kidney single cell datasets (KIT database) that support the findings of this study are openly accessible with following link: https://humphreyslab.com/SingleCell/.

ACKNOWLEDGMENTS

This research was supported by the Japan Agency for Medical Research and Development (AMED) under grant numbers AMED-CREST 23gm1210009 (MYan), 21gm5010002 (MYan), 23zf0127003h001 (MYan), 23ek0310020h0001 (MYan), and 22zf0127001 (TA); KAKENHI Grant-in-Aid (20H03697, 23H02925, 23K18288 to MYan); and Grant-in-Aid for Young Scientists (21K16162 to ShinY) from the Ministry of Education, Culture, Sports, Science, and Technology of Japan. This work was also supported by Japan Society for the Promotion of Science (JSPS) KAKENHI grant number JP16H06280; Grant-in-Aid for Scientific Research on Innovative Areas—Platforms for Advanced Technologies and Research Resources "Advanced Bioimaging Support"; the grants from the Uehara Memorial Foundation (MYan), the Takeda Science Foundation (MYan), the Sumitomo Foundation (MYan), and the Mochida Memorial Foundation for Medical and Pharmaceutical Research (ShinY); and the research grant from Gout and Uric Acid Foundation of Japan (ShinY) and Suzuken Memorial Foundation (ShinY). The authors are grateful to Professor Michiyuki Matsuda for valuable suggestions and guidance. This work was supported partly by the World Premier International Research Center Initiative (WPI), MEXT, Japan, and the Kyoto University Live Imaging Center. Part of this work was included as an abstract at the Annual Meeting of the American Society of Nephrology.

AUTHOR CONTRIBUTIONS

ShigY and MYan designed the experiments. ShigY, ShinY, and MYan wrote the manuscript. MYan supervised the project. ShinY, MT, AM, AO, SN, MYam, and ShigY performed the experiments. SF, NT, MYam, and ShigY analyzed the data. TA and HI provided the resources and reviewed and edited the manuscript.

Supplementary material is available online at www.kidney-international.org.

REFERENCES

1. Zhan M, Brooks C, Liu F, et al. Mitochondrial dynamics: regulatory mechanisms and emerging role in renal pathophysiology. *Kidney Int*. 2013;83:568–581.
2. Chung KW, Dhillon P, Huang S, et al. Mitochondrial damage and activation of the STING pathway lead to renal inflammation and fibrosis. *Cell Metab*. 2019;30:784–799.e5.
3. Maekawa H, Inoue T, Ouchi H, et al. Mitochondrial damage causes inflammation via cGAS-STING signaling in acute kidney injury. *Cell Rep*. 2019;29:1261–1273.e6.
4. Yamamoto S, Yamamoto M, Nakamura J, et al. Spatiotemporal ATP dynamics during AKI predict renal prognosis. *J Am Soc Nephrol*. 2020;31:2855–2869.
5. Lindsey ML, Bolli R, Canty JM, et al. Guidelines for experimental models of myocardial ischemia and infarction. *Am J Physiol Heart Circ Physiol*. 2018;314:H812–H838.
6. Weinberg JM, Venkatachalam MA, Roeser NF, Nissim I. Mitochondrial dysfunction during hypoxia/reoxygenation and its correction by anaerobic metabolism of citric acid cycle intermediates. *Proc Natl Acad Sci U S A*. 2000;97:2826–2831.
7. Karbach U, Kricke J, Meyer-Wentrup F, et al. Localization of organic cation transporters OCT1 and OCT2 in rat kidney. *Am J Physiol Renal Physiol*. 2000;279:F679–F687.
8. Filipski KK, Mathijssen RH, Mikkelsen TS, et al. Contribution of organic cation transporter 2 (OCT2) to cisplatin-induced nephrotoxicity. *Clin Pharmacol Ther*. 2009;86:396–402.
9. Ludwig T, Riethmüller C, Gekle M, et al. Nephrotoxicity of platinum complexes is related to basolateral organic cation transport. *Kidney Int*. 2004;66:196–202.
10. Nieskens TTG, Persson M, Kelly EJ, Sjögren AK. A multicompartment human kidney proximal tubule-on-a-chip replicates cell polarization–dependent cisplatin toxicity. *Drug Metab Dispo*. 2020;48:1303–1311.
11. Suzuki T, Yamaguchi H, Kikusato M, et al. Mitochonic acid 5 (MA-5), a derivative of the plant hormone indole-3-acetic acid, improves survival of fibroblasts from patients with mitochondrial diseases. *Tohoku J Exp Med*. 2015;236:225–232.

12. Suzuki T, Yamaguchi H, Kikusato M, et al. Mitochonic acid 5 binds mitochondria and ameliorates renal tubular and cardiac myocyte damage. *J Am Soc Nephrol*. 2016;27:1925–1932.
13. Wu H, Kirita Y, Donnelly EL, Humphreys BD. Advantages of single-nucleus over single-cell RNA sequencing of adult kidney: rare cell types and novel cell states revealed in fibrosis. *J Am Soc Nephrol*. 2019;30:23–32.
14. Heyman SN, Rosenberger C, Rosen S. Experimental ischemia-reperfusion: biases and myths-the proximal vs. distal hypoxic tubular injury debate revisited. *Kidney Int*. 2010;77:9–16.
15. Gerhardt LMS, Liu J, Koppitch K, et al. Single-nuclear transcriptomics reveals diversity of proximal tubule cell states in a dynamic response to acute kidney injury. *Proc Natl Acad Sci U S A*. 2021;118:e2026684118.
16. Conesa EL, Valero F, Nadal JC, et al. N-acetyl-L-cysteine improves renal medullary hypoperfusion in acute renal failure. *Am J Physiol Regul Integr Comp Physiol*. 2001;281:R730–R737.
17. Regner KR, Zuk A, Van Why SK, et al. Protective effect of 20-HETE analogues in experimental renal ischemia reperfusion injury. *Kidney Int*. 2009;75:511–517.
18. Vetterlein F, Pethö A, Schmidt G. Distribution of capillary blood flow in rat kidney during postischemic renal failure. *Am J Physiol*. 1986;251(Pt 2):H510–H519.
19. Eckardt KU, Bernhardt WM, Weidemann A, et al. Role of hypoxia in the pathogenesis of renal disease. *Kidney Int Suppl*. 2005;68(99):S46–S51.
20. Tanaka S, Tanaka T, Nangaku M. Hypoxia as a key player in the AKI-to-CKD transition. *Am J Physiol Renal Physiol*. 2014;307:F1187–F1195.